ISSN: 2688-8645

Thermal Management and Performance Validation of a High Temperature Downhole Monitoring System for Smart Well Applications

Yan Zheng, Long Wang *, Zhiqiang Dun, Junyu Zhong

School of Mechanical Engineering, Southwest Petroleum University, Chengdu, Sichuan 610500, China

* Correspondence Author: Long Wang

Abstract

To obtain environmental parameters of production zones during well completion operations, a high-temperature-resistant downhole multi-parameter monitoring system was designed. By enabling remote monitoring of downhole environmental parameters, the system provides a basis for formulating efficient extraction strategies. To address the challenge of electronic equipment failure under high temperatures, the heat transfer mechanism of circuits within the hermetically sealed environment of downhole electrically controlled flow control valves was analyzed. A thermal simulation model of downhole circuits was established, and thermal analysis of downhole acquisition circuits was conducted using specialized simulation software. Through optimized chip layout and heat dissipation design, the system's heat resistance was significantly improved. For communication, the Modbus protocol was selected, and a surface control system was developed using the ForceControl platform. This achieved real-time communication between surface control equipment and downhole acquisition circuits. Multi-node communication tests and high-temperature experiments verified that the monitoring system operates stably at 120°C, with accurate and reliable data transmission among multiple nodes, meeting actual engineering requirements. This system offers a reliable solution for the design of intelligent downhole multi-parameter monitoring systems.

Keywords

Downhole Parameter Acquisition; Remote Monitoring; Thermal Design; Modbus Communication Protocol; Thermal Reliability Testing.

1. Introduction

Against the backdrop of global technological advancement, technologies in the oil and gas industry are advancing toward digitalization, informatization, and intelligentization [1-2]. Intelligent Well Completion (IWC) is an optimized completion technology that integrates real-time monitoring of downhole environmental parameters, production analysis and decision-making, and remote control of downhole tools into a unified technical system for oil and gas wells [3-5]. The installation of permanent downhole sensors enables the continuous acquisition of critical downhole parameters - including pressure, temperature, flow rate, and water cut - which are transmitted in real-time to the surface control system. The production optimization system then integrates reservoir models with production objectives to formulate optimized production strategies and control protocols [6-8]. Based on analytical decision-making outputs, multi-position choking adjustments are dynamically executed on downhole inflow control valves (ICVs) to achieve precise regulation of flow and pressure parameters across multiple

ISSN: 2688-8645

target production zones. This real-time zonal management enhances hydrocarbon recovery efficiency while maintaining conformance with production optimization objectives [9-11].

The real-time downhole environmental parameter monitoring systems for intelligent wells confront significant technical challenges, including elevated temperatures, high-pressure conditions, stringent spatial constraints, and complex environment media [12]. Serving as core components of these downhole monitoring systems, electronic equipment exhibits reliability that fundamentally governs the operational lifespan of the entire monitoring infrastructure. According to statistical data, over 55% of electronic device failures are attributed to excessive operating temperatures [13]. To enhance the efficiency and reliability of oil and gas extraction, thermal design must be implemented for downhole measurement and control circuits. This requires developing effective thermal management strategies to ensure sustained system stability during long-term operation in high-temperature, high-pressure environments [14].

Globally, extensive research has been conducted on the operational stability and reliability of electronic devices in high-temperature environments. Zhang Jianwei et al. performed thermal simulation analysis on critical circuits of geothermal deep-borehole acoustic logging sensors, with the simulation results providing critical design guidelines for structural configuration optimization, circuit layout refinement, and other aspects [15] . Carlos Arroyo-Ruiz et al. optimized the thermal dissipation paths of space platform electronic equipment using thermal simulation analysis methods. Through coupled simulation analysis, they refined the PCB copper layer design and constructed optimal thermal paths, effectively improving the temperature distribution of electronic components on space platform PCBs[16]. Wenka Gao et al. addressed the thermal dissipation challenges in high-temperature well logging-while-drilling tools by designing an active cooling system based on split-type Stirling cryocoolers. They investigated key parameters closely related to cooling performance, achieving improved cooling effectiveness[17].

In the field of oil and gas extraction, substantial achievements have been made in the design of intelligent well-downhole parameter monitoring systems. Safaa Najah Saud Al-Humairi et al. developed a sensor network-based downhole parameter monitoring system that enables remote transmission of downhole data through communication networks, facilitating remote well health monitoring and reducing manual inspections [5]. Mei Wang et al. designed a multi-parameter monitoring system for oil wells capable of real-time downhole parameter measurement, demonstrating excellent scalability and reliability [9]. However, existing studies have predominantly focused on conventional operating conditions, with limited systematic investigation into the thermal design and optimization of monitoring systems for downhole high-temperature environments within structurally constrained spaces.

This study conducts targeted design for the special downhole environment characterized by spatial constraints and extreme high-temperature conditions. Emphasis is placed on enhancing the system's temperature resistance performance through optimized chip layout and improved heat dissipation methods. Functional correctness and operational reliability of the downhole multi-parameter monitoring system under actual working conditions are validated through high-temperature experiments.

2. Hardware Circuit and Working Principle

2.1. Principle of operation

The downhole parameters that need to be monitored in smart wells mainly include four categories: pressure parameters, temperature parameters, flow parameters, and equipment parameters. Pressure parameters involve monitoring tubing pressure, casing pressure, and formation pressure, which are used to evaluate the productivity and operating status of oil wells. Temperature parameters require monitoring reservoir temperature, wellbore

ISSN: 2688-8645

temperature, and annulus temperature, serving to determine reservoir fluid properties and equipment operating conditions. Flow parameters entail monitoring oil well fluid production, water cut, and sand content, which are utilized to identify indicators of oil well productivity. Equipment parameters involve monitoring the operating status of various downhole equipment, including motor speed, central pipe opening degree, etc., facilitating the timely detection of faults and abnormalities for maintenance and repair.

Considering the characteristics of dense sensor placement and wide spatial coverage in downhole monitoring systems, combined with spatially constrained downhole structural conditions, the system employs a distributed modular architecture design. Synchronous measurement of multiple downhole parameters is achieved through multi-node collaborative communication protocols. The downhole parameter monitoring system employs a distributed architecture to achieve multi-parameter acquisition. This paper focuses on constructing a real-time monitoring system for temperature and pressure parameters, utilizing external pressure and temperature sensors to collect downhole environmental temperature and pressure data. A surface high-temperature test platform is constructed to validate the functionality and reliability of the monitoring system. Sensors for monitoring parameters such as water cut, sand content, and flow rate can be directly connected to the acquisition interface in subsequent practical applications.

The functional logic diagram of the downhole parameter monitoring system is shown in Fig 1. Permanent downhole sensors collect temperature and pressure parameters in real time. The acquired analog signals are converted into digital signals via an ADC (Analog-to-Digital Converter) chip and stored in the main controller. Upon receiving a data request from the surface control equipment, the main controller compiles the stored information into a Modbus-RTU protocol data frame. This frame is transmitted to the surface control system via the communication module, where it is parsed and displayed in real time. Power is supplied to the downhole circuitry from the surface equipment through a cable. After step-down voltage regulation and stabilization by the DC-DC power module, the power is distributed to components on the PCB.

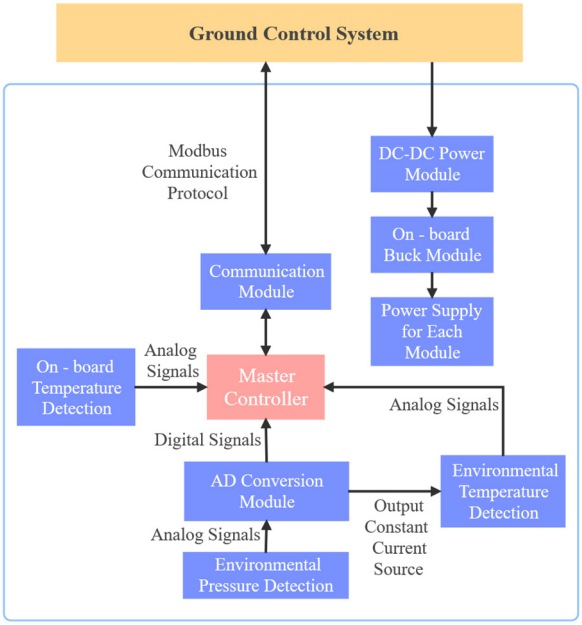

Fig 1. Operation logic diagram of the downhole parameter monitoring system

ISSN: 2688-8645

3. Thermal Transfer Mechanism and Thermal Simulation Analysis

3.1. Downhole Circuit Heat Transfer Model

This paper conducts PCB thermal design from two aspects: thermal radiation from the environment and affected by the self-heating of the PCB. It performs an in-depth analysis of the environmental temperature's impact on the thermal radiation affecting the PCB, serving as the basis for thermal design.

The PCB circuit board of the parameter monitoring system is installed in the electronic sealing chamber of the electrically controlled flow control valve, located between the main valve body and the central tube. The fluid medium within the sealing chamber is air. During the operation of the electronically controlled flow control valve, its position basically does not change, and its temperature can be considered equivalent to the environmental temperature of the surrounding wellbore. The electronic sealing chamber undergoes sealing and pressure isolation treatment, ensuring the internal fluid temperature matches the environmental temperature. The parameter monitoring system must maintain stable performance in high-temperature environments, with thermal simulation analysis conducted under environmental temperatures of 120°C. The electronically controlled flow control valve features an outer diameter of 114 mm and an inner diameter of 46 mm. The annular space is extremely narrow, resulting in severely limited space available for printed circuit board placement. The mounting position of the printed circuit board is shown in Fig 2, with PCB dimensions constrained to 23 mm × 150 mm.

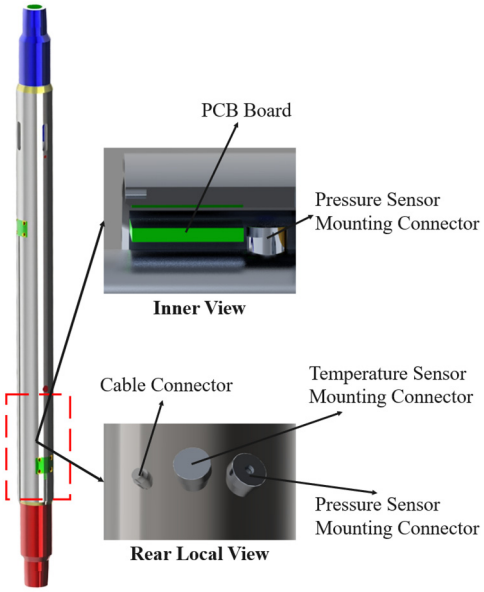

Fig 2. Schematic diagram of the installation location of the downhole circuit

3.2. Mechanism of Heat Transfer

Under high-temperature operating conditions in deep wells, the temperature rise of electronic components is influenced by the dual effects of external environmental heat transfer and self-healing. This temperature increase results from the coupled effects of multiple heat transfer mechanisms, including conduction, radiation, and convection [18-19] . The process involves internal conduction within the PCB, convection between the PCB and the surrounding air, radiation between the PCB and the isolation chamber walls, and convection between the air and the isolation chamber walls. The heat transfer model of the circuit board is illustrated in **Fig 3**, Where Q_{RA} represents heat radiation, Q_{CD} denotes heat conduction, and Q_{CV} indicates heat convection.

ISSN: 2688-8645

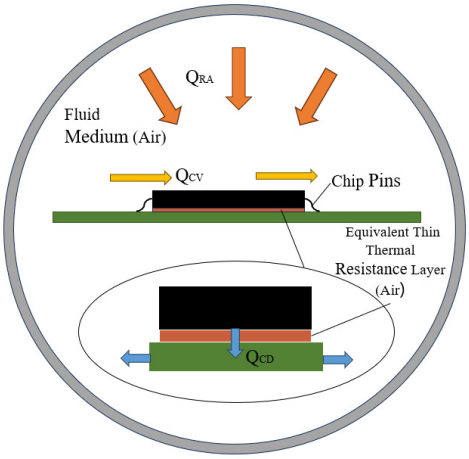

Fig 3. PCB board heat transfer model

Considering the coupled effects of conduction, convection, and radiation, a heat transfer model for downhole circuits is established. By analyzing the temperature distribution within the PCB under the influence of its thermal conductivity and internal heat sources, the internal conduction of the PCB is described as shown in Eq.(1), where k_{PCB} represents the anisotropic thermal conductivity of the PCB, T_{PCB} represents the internal temperature field of the printed circuit board, and Φ denotes the internal heat source.

$$\nabla \cdot \left(k_{PCB} \nabla T_{PCB} \right) + \dot{\Phi} = 0 \tag{1}$$

To determine the thermal exchange boundary conditions between the air, the PCB surface, and the chamber walls: The convective heat transfer between the air and the isothermal chamber walls is described as shown in Eq.(2). The heat flux on the PCB surface is equivalent to the sum of convective and radiation heat dissipation, as shown in Eq.(3). Where T_{air}-T_{wall} represents the temperature difference between the air and the chamber wall, T_{PCB}-T_{air} denotes the temperature difference between the PCB surface and the air, and T_{PCB}-T_{wall} indicates the temperature difference between the PCB surface and the chamber wall, k_{air} is the thermal conductivity of air, h_{wall} is the convective heat transfer coefficient between the chamber wall and the air, h_{conv} is the convective heat transfer coefficient between the PCB surface and the air, $\in$is the emissivity of the PCB surface, and σ is the Stefan-Boltzmann constant.

$$-k_{air} \frac{\partial T_{air}}{\partial n} = h_{wall} (T_{air} - T_{wall}) \tag{2}$$

$$-k_{PCB} \frac{\partial T_{PCB}}{\partial n} = h_{conv} (T_{PCB} - T_{air}) + \int \sigma \left(T_{PCB}^4 - T_{wall}^4 \right) \tag{3}$$

Considering buoyancy-driven convective flow, the natural convection of air within an enclosed chamber induced by temperature differences is described by Eq.(4). The convective heat transfer and energy balance of air are formulated in Eq.(5). The calculation procedure for the volumetric heat source Q_{source} is detailed in Eq.(6). In these equations: ρ_0 denotes the air density, μ represents the dynamic viscosity, g corresponds to the gravitational acceleration, β signifies the thermal expansion coefficient, j is the unit vector in the vertical direction, c_p indicates the specific heat capacity at constant pressure, V_{cell} represents the differential volume element.

$$\rho_0 (v \cdot \nabla) v = -\nabla p + \mu \nabla^2 v + \rho_0 g \beta (T_{air} - T_{wall}) j \tag{4}$$

$$\rho_0 c_p v \cdot \nabla T_{air} = \nabla \cdot \left(k_{air} \nabla T_{air} \right) + Q_{source} \tag{5}$$

ISSN: 2688-8645

$$Q_{source} = \frac{1}{V_{cell}} \int_{PCB} h_{conv} (T_{PCB} - T_{air}) dA \tag{6}$$

The PCB board typically consists of multiple alternating layers of copper foil and FR-4 substrate, exhibiting anisotropic thermal conduction properties. For the hybrid structure of a single copper layer and FR-4, the equivalent thermal conductivity is described as shown in Eq.(7). Among them, k_i represents the equivalent thermal conductivity of the composite material, α represents the layer coverage rate of copper, k_{Cu} represents the thermal conductivity of copper, and k_{FR4} represents the thermal conductivity of the dielectric material.

$$k_i = \alpha k_{Cu} + (1-\alpha) k_{FR4} \tag{7}$$

For multilayer PCBs, heat transfer in the in-plane direction is dominated by the high thermal conductivity of copper layers. Given a total PCB thickness d, containing n copper layers, each with thickness δ_i, the in-plane equivalent thermal conductivity k_{in} is given by Eq.(8).

$$k_{in} = \left[\sum_{i=1}^{n} \delta_i k_i + \left(d - \sum_{i=1}^{n} \delta_i \right) k_{FR4} \right] \Big/ d \tag{8}$$

The heat flow in its surface normal direction perpendicularly passes through each layer, and the equivalent thermal conductivity in the normal direction, k_{nor}, is given by Eq.(9).

$$k_{nor} = d \Big/ \left[\sum_{i=1}^{n} \delta_i / k_i + \left(d - \sum_{i=1}^{n} \delta_i \right) / k_{FR4} \right] \tag{9}$$

3.3. Simulation Analysis of Heat Transfer

Thermal analysis of the PCB is conducted using thermal simulation software, employing coupled simulations of multiple heat transfer mechanisms: thermal conduction, thermal radiation, and thermal convection.

During the construction of the thermal simulation model, structures with minimal impact on heat dissipation are simplified, and small-sized components with negligible power consumption are omitted after evaluating their thermal influence. This approach ensures no significant loss of computational accuracy while substantially reducing model complexity. After simplification and exclusion of low-power components, the reduced PCB model for thermal simulation is depicted in **Fig 4**.

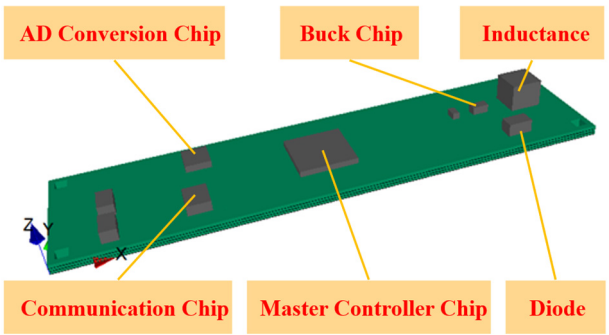

Fig 4. Thermal simulation PCB board simplified model

On the top signal layer of a PCB, areas with copper pours and trace routing exhibit lower thermal resistance compared to regions without copper coverage. To effectively enhance the accuracy of thermal simulation calculations, these two distinct regions should be partitioned into separate zones.

ISSN: 2688-8645

The thermal simulation is then performed under an environmental temperature of 120℃. In this scenario, the boundary temperature for thermal simulation is set to 120℃, while the fluid medium inside the isolation chamber is defined as 120℃ air. The simulation results are shown in **Fig 5**. As indicated, the maximum surface temperature of the PCB reaches 136.9℃, with the hottest point still located at the DC-DC buck converter chip. Temperatures of other chips remain below 130℃.

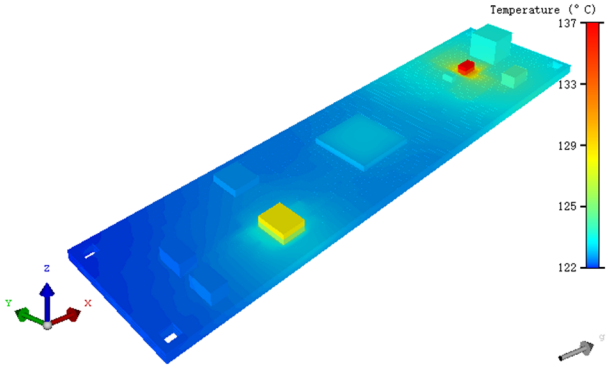

Fig 5. Schematic diagram of the surface temperature of the PCB board in the 120℃ thermal simulation

4. Optimization of Thermal Design Scheme

4.1. Optimization Strategies

The thermal simulation results indicate that the operating temperatures of all chips remain within their maximum operating temperature ranges, validating the rationality of the circuit design and meeting the predetermined design requirements. Given the inevitable discrepancies between thermal simulation results and actual measurements, coupled with the significant impact of high-temperature environments on the reliability of electronic components, further optimization of the PCB circuit design and thermal management methods becomes particularly necessary. The ambient temperature of the optimization scheme is set at 120℃, and the optimization work is mainly carried out from two aspects: the optimization of the chip layout and the optimization of the heat dissipation method. The thermal design optimization work will be promoted around the point with the highest temperature. From the thermal simulation analysis results presented in Section 3.3 of this paper, the DC-DC buck converter chip is at the point with the highest temperature, and the temperature at this chip is the core concern of heat dissipation optimization.

4.2. Chip Layout Optimization

When the position of chips on the PCB is altered, both the thermal conduction paths and convective heat transfer efficiency will change accordingly. To analyze temperature variations of the DC-DC buck converter chip at different PCB locations, detailed thermal simulations are conducted to determine the optimal circuit layout. During these simulations, variations in thermal conductivity across regions caused by differing copper-clad areas on signal layers during modeling may interfere with simulation results. To control variables in thermal simulations and eliminate such interference, large-area uniform copper cladding should be applied to the signal layers[20]. Compared to the thermal simulation results in section 3.3, this uniform copper cladding reduces the overall temperature of the PCB. However, this outcome serves only as a reference for chip layout optimization.

A coordinate system is established with the lower-left corner of the printed circuit board as the origin, aligning the long side with the X-axis and the short side with the Y-axis. This configuration is used to investigate the relationship between chip temperature and positions

ISSN: 2688-8645

along the X- and Y- axes. **Fig 6** illustrates the relationship between the maximum temperature on the printed circuit board and position variations along the X- and Y-axes. As shown, when the Y-axis position remains constant, the fluctuation of the highest PCB temperature along the X-axis is less than 0.1℃. This indicates that the chip temperature is minimally influenced by the X-axis position. Therefore, the DC-DC buck converter chip can be placed at the edge of the PCB to reduce electromagnetic interference with other modules. When the position on the X-axis remains constant, the position of the highest PCB temperature varies significantly with the Y-axis position. When the chip's position is between 9 mm and 18 mm, the temperature fluctuation is within 0.2 ℃, with a relatively small variation range. This small variation suggests that this range is an optimal area for chip placement.

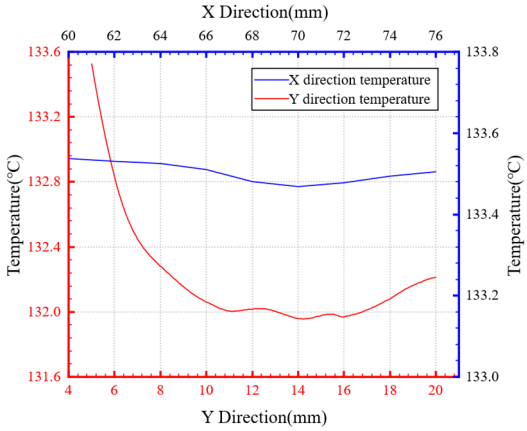

Fig 6. Relationship diagram between the chip temperature and its position

4.3. Optimization of Heat Dissipation Design

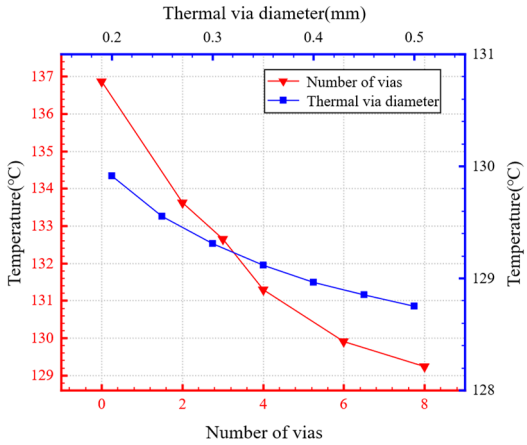

Fig 7. Influence of the number of heat dissipation vias and via diameter on the temperature

Thermal management design employs two heat dissipation methods: placing thermal vias beneath the chip and incorporating heat sinks. The thermal vias are specified with a diameter of 0.2 mm and a spacing of 1 mm. Additionally, the PCB backplate is connected to the heat sink, with thermal grease applied between their interfaces to enhance thermal conductivity. The heat sink adopts a finned design. Due to space constraints within the electronic sealing chamber, its dimensions are as follows: a height of 4.3 mm, a base thickness of 1.7 mm, an initial fin width of 0.7 mm, and an initial fin count of 7 fins. The heat sink is fabricated from 6063 aluminum alloy. The number and diameter of thermal vias significantly influence thermal resistance [21-23]. Here, we analyze the impact of thermal via quantity and diameter on the maximum temperature

ISSN: 2688-8645

point of the PCB. As shown in **Fig 7**, when the thermal via diameter is fixed at 0.2 mm, increasing the number of vias gradually reduces the PCB's highest temperature. However, as the number continues to grow, the rate of temperature reduction gradually slows. Considering factors such as the bottom area of the DC-DC buck converter chip, the optimal number of thermal vias is determined to be 6. With the number of vias fixed at 6, the PCB's maximum temperature also decreases as the diameter of the vias increases. After a comprehensive evaluation, a diameter of 0.3 mm is selected for the thermal vias.

The optimization design of the fin structure selects the fin width and fin count as design variables, with the objective of minimizing the temperature rise at the PCB's highest temperature point. Parametric optimization is performed, and the relevant simulation results are shown in **Fig 8**.

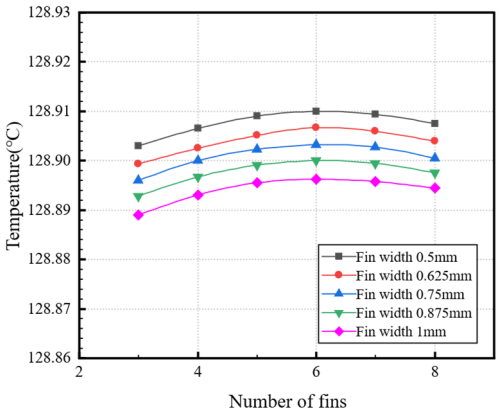

Fig 8. Influence of the number of fins and fin width on temperature

The simulation results show that variations in the fin count and thickness of the heat sink fins have less than a 0.1℃ impact on the maximum temperature point of the PCB. Analysis indicates that this is primarily due to the thermal conduction efficiency in the system being constrained by the previously configured thermal vias. Therefore, the heat sink fins can be selected from commercially available off-the-shelf products without requiring specialized customization. Combining all optimization schemes, the final optimized results, as shown in **Fig 9**, achieve a maximum PCB temperature of 128.9℃, representing an 8℃ reduction compared to the pre-optimization scenario. This improvement effectively enhances the thermal endurance performance of the monitoring system, ensuring more reliable operation under elevated temperatures.

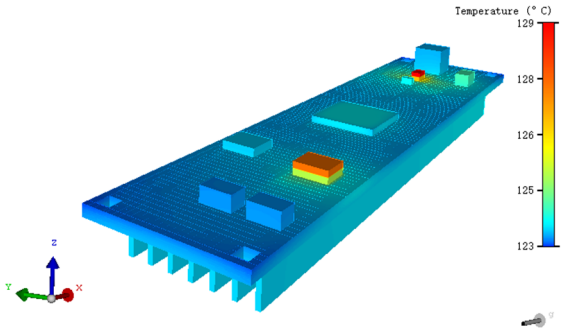

Fig 9. PCB thermal design optimization thermal simulation diagram

ISSN: 2688-8645

5. Program Design and Experimental Testing

5.1. Experimental Testing and Analysis

To verify the high-temperature stability and measurement accuracy of the real-time downhole environmental parameter monitoring system, joint debugging under simulated actual operating conditions was conducted on the entire system. The optimized printed circuit board for the downhole acquisition circuit is shown in **Fig 10**.

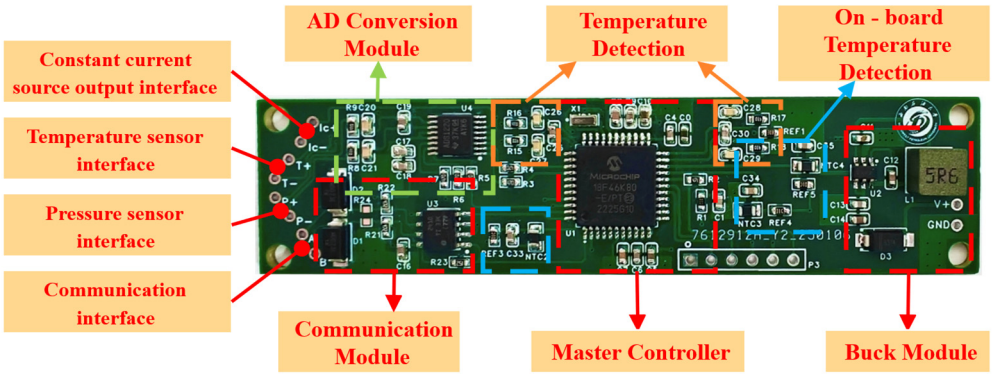

Fig 10. Physical diagram of the PCB board

To validate the multi-node acquisition function of the downhole monitoring system, the upper computer established synchronous connections with three monitoring nodes via the RS-485 bus for communication testing, a configuration shown in **Fig 11**. During 10-hour continuous operation, all nodes maintained stable uploads of environmental parameter data packets at 952ms intervals. All frames passed CRC checks with a bit error rate (BER) below 1×10^{-9}. The multi-node communication process proceeded without errors, ensuring accurate data transmission, which confirms the system's reliable multi-node communication capability.

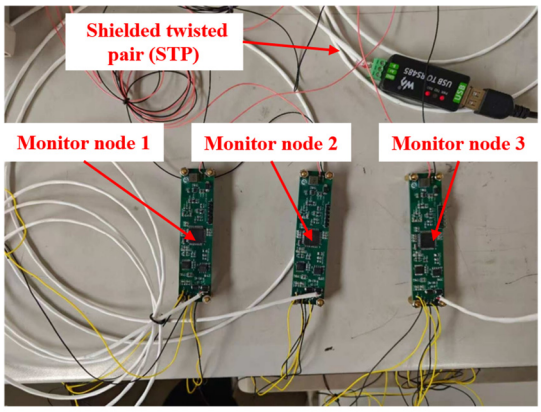

Fig 11. Multi-node communication test

During high-temperature testing, the PCB board of the downhole circuit was placed in a constant-temperature oven for heating. The oven employed non-linear heating with a target temperature of 120°C, and the heating process was sustained for 24-hour to evaluate the stability of the circuit under prolonged high-temperature conditions. Simultaneously, all sensors were positioned within the same testing environment to enable real-time monitoring. The setup of the constant-temperature oven used in this experiment is illustrated in **Fig 12**.

Three temperature sensors mounted on the PCB were used to monitor the temperatures of major heat-generating areas on the PCB board in real time. A PT1000 temperature sensor was installed inside the constant-temperature oven to continuously monitor the ambient

ISSN: 2688-8645

temperature. A pressure sensor was installed on the flow control valve. The pressure test was carried out with a hydraulic station, which pressurized the system to 40 MPa before it stabilized. After a period of stabilization, the pressure was gradually released. The entire testing process was recorded in real time by the downhole parameter monitoring system. The actual testing setup is shown in **Fig 13**. After 24-hour of continuous high-temperature testing at 120°C, the downhole circuit functioned normally throughout the test and retained its normal functionality post-test, demonstrating the high reliability of the downhole parameter monitoring system under 120°C high - temperature conditions.

Fig 12. Constant temperature chamber test diagram

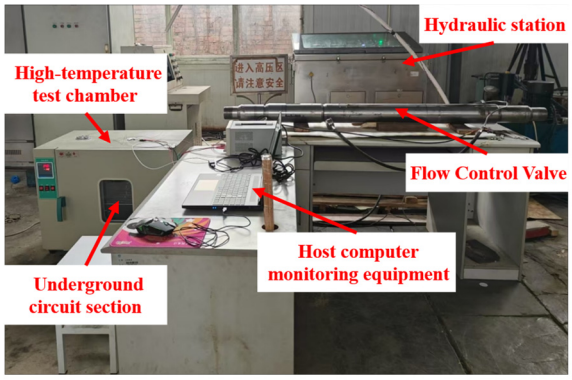

Fig 13. Actual test working diagram

After the parameters collected by the downhole circuit are transmitted to the host computer, the computer performs post-processing on the returned data. The processed data is then visualized and displayed on the monitoring interface, as shown in **Fig 14**. Following multi-node communication testing and high-temperature trials, the system's capability to collect environmental parameters from multiple downhole nodes in real time has been validated.

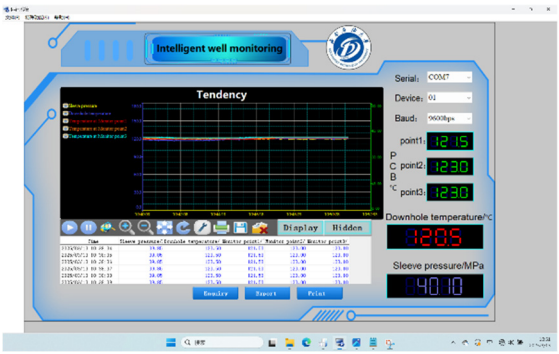

Fig 14. Host computer monitoring interface

ISSN: 2688-8645

To validate the accuracy of the system, some data collected by the host computer during high-temperature testing was exported and analyzed. As shown in **Fig 15**, the downhole parameter monitoring system can accurately acquire environmental parameters under high-temperature conditions and transmit them back to the ground control system. The returned data varies in line with the operational patterns of the equipment, which validates the system's real-time performance and accuracy.

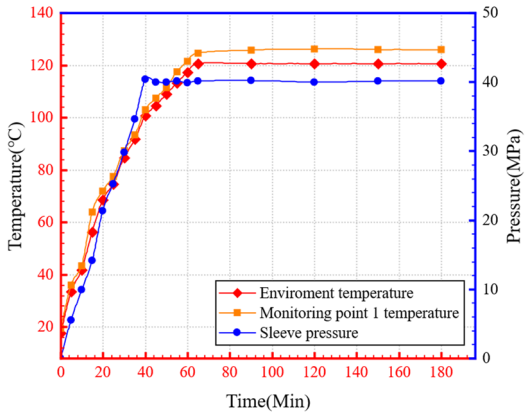

Fig 15. Data curve of environmental parameter acquisition

6. Conclusion

In response to the requirements for real-time monitoring of downhole production zone environmental parameters in intelligent well-completion operations, a multi-parameter real-time monitoring system suitable for high-temperature environments has been successfully developed. To address the special working conditions of high temperature, confinement, structurally confined downhole space, and natural heat dissipation downhole, in-depth research has been conducted on thermal analysis and optimal design of downhole high-temperature circuits, effectively solving the thermal management challenges in high-temperature confined downhole environments. The main research findings are as follows:

1. Thermal simulation software was employed to conduct thermal analysis of the downhole circuit section. The results demonstrate that under operating conditions with an ambient temperature of 120°C, the highest temperature area on the circuit board reaches 136.9°C, with the DC-DC step-down chip location exhibiting the maximum temperature.
2. Based on simulation results, thermal optimization design was performed on the downhole circuit section. Through rational optimization of circuit layout and improvement of heat dissipation methods, the maximum temperature of the circuit board was reduced by 8°C, significantly enhancing the high-temperature resistance performance of the downhole circuit.
3. After undergoing a 10-hour multi-node communication test and a 24-hour high-temperature test at 120°C, the parameter monitoring system operated stably with all functions performing normally. Verification confirms that this monitoring system demonstrates outstanding characteristics including high measurement accuracy, strong real-time performance, and excellent reliability in high-temperature environments, fully meeting the monitoring requirements for downhole high-temperature conditions.

ISSN: 2688-8645

Acknowledgments

The authors sincerely acknowledge the financial support from the General Program of Sichuan Natural Science Foundation (Grant No. 2022NSFC0402).

References

[1] Li, G., Song, X., Zhu, Z., Tian, S., & Sheng, M. (2023). Research progress and prospect of intelligent well-completion technology. Oil Drilling Technology, 51, 35–47.

[2] Afuekwe, A., & Bello, K. (2019). Use of smart controls in intelligent well completion to optimize oil & gas recovery. Engineering Research and Reports, 5, 1-14.

[3] Luo, J., He, D. S., Zheng, J. L., Xiong, L., Li, R. L., & Luan, J. S. (2023). Research progress in downhole electric flow control technology in China and abroad. China Petroleum Machinery, 51(10), 77-84, 156.

[4] Raufi, M. H., Masihi, M., Behrouz, T., & Keshavarz, N. (2014). Statistical analysis of the added value by intelligent well application under reservoir uncertainty. Energy Sources, Part A: Recovery, Utilization, and Environmental Effects, 36(22), 2449-2457. https://doi.org/10.1080/ 15567036. 2011.572122.

[5] Al-Humairi, S. N. S., Tarshen Ravindran, D. R., Abdullah, M. I., Hamzah, B., & Alkawaz, M. H. (2020). Intelligent Monitoring System for Oil Well Efficiency. 2020 16th IEEE International Colloquium on Signal Processing & Its Applications (CSPA), 13–17. https://doi.org/10.1109/ CSPA48992. 2020. 9068668.

[6] Feng, G., Yin, Y., Ma, L., Zhang, L., & Wang, W. (2022). Development and application of intelligent well technology in offshore oilfield. Journal of Southwest Petroleum University (Natural Science Edition), 44, 153-164.

[7] Schaefer, B. da Cruz, & Sampaio, M. A. (2020). Efficient workflow for optimizing intelligent well completion using production parameters in real-time. Oil & Gas Science and Technology - Revue d'IFP Energies nouvelles, 75, 69. https://doi.org/10.2516/ogst/2020061.

[8] Malakooti, R., Ayop, A. Z., Maulianda, B., Muradov, K., & Davies, D. (2020). Integrated production optimisation and monitoring of multi-zone intelligent wells. Journal of Petroleum Exploration and Production Technology, 10, 159-170. https://doi.org/10.1007/s13202-019-0719-5.

[9] Wang, M., Liang, L., Chen, K., & Wang, N. (2011). Design of the Oil Well Multi-Parameter Monitoring System. Advanced Materials Research, 383–390, 3652–3656. https://doi.org/10.4028/ www. scientific. net/AMR.383-390.3652.

[10] Wang, D., He, R., Han, J., Fattouche, M., & Ghannouchi, F. M. (2012). Sensor network based oilwell health monitoring and intelligent control. IEEE Sensors Journal, 12(5), 1326-1339. https://doi.org/ 10. 1109/JSEN.2011.2170411.

[11] Bouldin, B., Verma, C., Bellaci, I., Black, M., Dyer, S., Algerøy, J., De Oliveira, T., & Pan, Y. (2014). Prototype Test of an All-Electric Intelligent-Completion System for Extreme-Reservoir-Contact Wells. SPE Drilling & Completion, 29(3), 353–362. https://doi.org/10.2118/166507-PA.

[12] Ge, S. A., Ye, H., & Ma, Z. S. (2023). Construction of an online energy efficiency monitoring information system for major energy-consuming equipment in oil fields. Information System Engineering, (5), 49-51.

[13] Qi, W. L., Zhao, L., Wang, W. R., et al. (2022). Research progress of high heat flux electronic devices liquid cooling technology. Science Technology and Engineering, 22(11), 4261-4270.

[14] Jose, J., & Kumar Hotta, T. (2024). Thermal performance analysis and optimization of a heat pipe-based electronic thermal management system using experimental data-driven neuro-genetic technique. Thermal Science and Engineering Progress, 54, 102860. https://doi.org/10. 1016/j. tsep. 2024. 102860.

[15] Zhang, J. W., Yang, Z. J., Wang, X. J., et al. (2023). Thermal design of ultrasonic logging sensors for deep geothermal wells. Science Technology and Engineering, 23(1), 165-172.

ISSN: 2688-8645

[16] Arroyo-Ruiz, C., González-Barcena, D., González-Monge, J., & Sanz-Andrés, A. (2024). Conductive paths generation using topology optimization for worst-case thermal design in space systems. Advances in Space Research. Advance online publication. https://doi.org/10.1016/ j.asr. 2024. 10.029.

[17] Gao, W., Liu, K., Dou, X., Tang, S., & Zhang, L. (2021). Numerical investigation on cooling effect in the circuit cabin of active cooling system of measurement-while-drilling instrument based on split-Stirling refrigerator. Case Studies in Thermal Engineering, 28, 101621.https:// doi.org/ 10. 1016/ j. csite.2021.101621.

[18] Hörmann, P., Stelzl, D., Lichtinger, R., Van Nieuwenhove, S., Mazón Carro, G., & Drechsler, K. (2014). On the numerical prediction of radiative heat transfer for thermoset automated fiber placement. Composites Part A: Applied Science and Manufacturing, 67, 282-288. https://doi.org/ 10. 1016/ j.compositesa.2014.08.019.

[19] Yang, S., & Tao, W. (2019). Heat transmission science (5th ed.). Higher Education Press.

[20] Goksu, O. F., Bulut, E. B., Gulbahce, M. O., & Dusmez, S. (2024). Thermal design and performance evaluation of GaN power stage in a 4-level totem-pole PFC. AEU - International Journal of Electronics and Communications, 173, 154981.https://doi.org/10.1016/j.aeue.2023.154981.

[21] Zhang, H., Wang, W., & Deng, J. (2022). Optimal design of heat dissipation on low power PCB. Ferroelectrics, 595(1), 47–59. https://doi.org/10.1080/00150193.2022.2079455.

[22] Smarra, D. A., & Chodavarapu, V. P. (2021). Experimental Study of Thermal Management Characteristics of Mass via Arrays. Electronics, 10(9), 1027.https://doi.org/ 10.3390/ electrics 10091027.

[23] Yuan, Z., Ding, D., & Zhang, W. (2023). Effect of Thermal via Design on Heat Dissipation of High-Lead QFN Packages Mounted on PCB. Applied Sciences, 13(23), 12653. https://doi.org/ 10.3390/ app13 2312653.